Desalination and Water Treatment
www.deswater.com

doi:10.5004/dwt.2019.23521

148 (2019) 162–169
April

Metronidazole in aqueous solution removal by activated carbon fiber adsorption of systems: adsorption kinetics, adsorption isotherms and thermodynamics

Yu Gao[a], Yuzhi Liu[a], Danwa Zou[b], Heda Guan[a], Donglei Zou[a,*]

[a]*Jilin University, Key Laboratory of Groundwater Resources and Environment, Ministry of Education, Jiefang Road 2519, Jilin, 130000, China, Tel. 155-0021-2126, email: yugao16@jlu.edu.cn (Y. Gao), Tel. 180-0436-9356, email: yuzhishijie@qq.com (Y. Liu), Tel. 186-4538-2596, email: 543418303@qq.com (H. Guan), Tel. 135-0441-9315, email: zoudl@jlu.edn.cn (D. Zou)*

[b]*China Energy Conservation And Environmental Protection (CECEP) L&T Environmental Technology Co., Ltd, 100091, China, Tel. 152-1022-0515, email: zoudanwa19@163.com (D. Zou)*

Received 8 June 2018; Accepted 24 November 2018

ABSTRACT

Metronidazole (MNZ), as a widely used nitroimidazolehas various effects on the human body. In this study, metronidazole removal by activated carbon fibers (ACFs) was investigated. The influences of adsorption temperature, adsorption time and the pH of MNZ solution have been studied and the best conditions were determined. ACFs with high BET surface area of 175.40 m^2/g and 0.35 cm^3/g total pore volume has been obtained from these precursors. The analyses of kinetic data showed that the adsorption of MNZ on ACFs follows closely the pseudo-second order kinetic model. Analysis data of MNZ were analyzed by Langmuir, Freundlich isotherms and the best correlation was achieved by the Langmuir isotherms. Results of thermodynamic studies showed endothermic, spontaneous nature and chemisorption of MNZ adsorption on ACFs.

Keywords: Metronidazole; Activated carbon fiber; Adsorption kinetics; Adsorption isotherms; Thermodynamics

1. Introduction

Nitroimidazoles are classified as emerging contaminates due to their wide usage as antibiotics in human beings and as veterinary medicine additives in poultry and fish feed, leading to their detection in wastewaters from hospitals, pharmaceutical industries and fish-farms [1,2]. Metronidazole (MNZ) is a first-generation nirtroimidazole derivatives with high bactericidal activity against trichomonas, viscount organisms, anaerobic bacteria, giardiasis, protozoan and amoebiasis [3,4]. MNZ has various effects on the human body. For example, the increase of MNZ level has been found to be potentially carcinogenic and mutagenic [5]. The MNZ has attracted more attention because it is highly soluble, non-biodegradable and carcinogenic [6]. It has been detected in hospital effluent wastewaters at concentrations of 1.8–9.41 g/L [7]. MNZ has a chemical formula of $C_6H_9N_3O_3$ with a very high solubility (10.5 g/L at 298K) and molecular weight (171.15 g/mol) [8] in water, and is expected to be highly mobile in aqueous systems [9]. The structure of MNZ is shown in Fig. 1.

Due to the increasing interest in the removal of antibiotics from aqueous systems, several researchers explored the possibility of MNZ removal by some process. Lam et al. [10] studied the adsorption of MNZ on clinoptilolite by means of computational simulation. Johnson et al. [11] degraded MNZ in aqueous solution by UV/H_2O_2 process in single and multi-lamp tubular photoreactors, the maximum removal of MNZ were 13% and 41% for the single-lamp and multi-lamp photoreactors, respectively. Dantas et al. [4] studied direct photolysis of MNZ in aqueous solution promoted by ultra violet radiation. Ding et al. [12] studied adsorption of MNZ in aqueous solution by Fe-modified sepiolite. It was found that the Fe-modified sepiolite had higher adsorption capability (36.5%) for MNZ than that of others. Ahmed et al. [13,14] studied the sorption of

*Corresponding author.

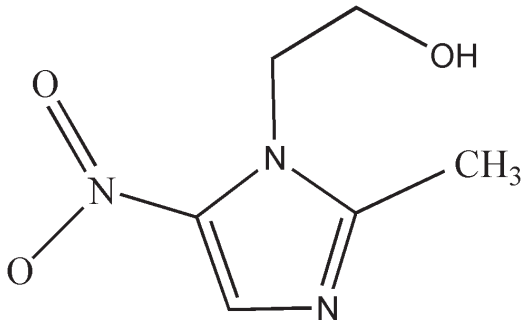

Fig. 1. Chemical structure of MNZ.

a nitroimidazole antibiotic, MNZ, onto such carbon from *Siris* seed pods has been investigated. Habibi et al. [15] used activated carbon removal metronidazole from aqueous solution. Mansur et al. [16] investigated the efficiency of MNZ removal utilizing light-weight expanded clay aggregates (LECA) and LECA coated with MgO nanoparticles (MgO/LECA). Çalışkan et al. [17] studied adsorption characteristics of sulfamethoxazole and metronidazole on activated carbon and it is concluded that activated carbon can be used to remove sulfamethoxazole and metronidazole from aqueous solutions. The adsorption of MNZ on activated carbon is physical in nature. The experimental adsorption data showed good correlation with the Langmuir isotherm model. Therefore, over the past few years they are considered to be an emerging environmental problem and it has been necessary to remove these contaminants from aqueous systems.

Activated carbon fiber (ACF), as a kind of promising adsorption material and novel adsorbents of high efficiency, can be widely used for treatment of organic wastewater, air purification and catalysis support [18,19]. Comparing with the other forms of activated carbon, such as powder activated carbon and granular activated carbon, activated carbon fibers (ACFs) have many favorable characteristics including high adsorption capacities and high mass transfer rates for both adsorption and desorption. ACF is much more popular for the benefits of easy processing and fast adsorption kinetics [20,21].

The aim of this work is to study the use of ACFs as an adsorbent for the removal of MNZ from aqueous solutions. The effects of the adsorbent dose, pH, temperature, equilibrium time, adsorption kinetics and adsorption isotherm were investigated. For evaluating various kinetics and adsorption parameters of the adsorption process, we attempted to apply the adsorption rate expression model to the current study and the results were discussed.

2. Materials and methods

2.1. Materials

ACFs used in this study were obtained from Shenyang Carbon Fiber Corporation (Jilin Province, China). MNZ (supplied by Rubio Company, China) of purity 98.0% and molecular weight of 171.15 g/mol was used as an adsorbate. All other chemicals used such as hydrochloric acid and NaOH were of analytical grades. Deionized water was used throughout the experiment.

2.2. Preparation and Characterization

The ACFs were boiled, washed three times in distilled water and dried at 338 K for 1 h before being used as adsorbent. ACFs were cut into pieces (2 cm × 2 cm). Batch adsorption experiments were performed at different temperatures (25°C, 30°C, 35°C) in a set of Erlenmeyer flasks (250 mL), each contains 150 mL of different concentrations (10 mg/L, 20 mg/L and 30 mg/L), together with 1.0 g ACF samples. Subsequently, Erlenmeyer flasks were kept in a temperature-controlled incubator shaker at 25°C with continuous shaking at 160 rpm for different adsorption time. Each experiment was repeated under identical conditions.

The pH of the solution was adjusted using the PhS-25 meter (Shanghai Jingmi Company, China) with a 6 mol L^{-1} NaOH and /or a 4 mol L^{-1} HCl. The mixtures were shaken in a thermostatic shaker bath (ZWY-100H/240 mechanical shaker, Shanghai Zhicheng Annlytical Instrument Manufacturing Co., Ltd, China) at desired temperature and contact time, and then the MNZ aqueous solution were filtered by membranes (0.22 μm). For characterization of the MAC, the morphology and elemental composition of the MAC was observed with a JEOL 5800 (Japan) scanning electron microscopy (SEM) at 20 kV. The brunauerемmett teller (BET) surface area, average pore size distribution was estimated using the surface area analyzer made by Quantcahrome Instruments. USA.

The absorbance of the MNZ aqueous solution was analyzed using a UV–vis spectropho-tometer (UV2600, Shanghai Shunyu Company, China) at its maximum absorption wavelength of 319 nm. MNZ concentrations were calculated by the adsorption calibration curve of MNZ aqueous solution (y = 0.571x–0.0402, R^2 = 0.9999). The adsorption capacity of the composites was calculated using Eq. (1).

$$q_e = \left(C_0 - C_e\right)V / W \tag{1}$$

where C_0 and C_e are MNZ concentrations at the start of the experiment and at equilibrium (mg/L), respectively. V (L) is the volume of MNZ solution and W (g) is the mass of adsorbent.

$$MNZ\ removal\ (\%) = \left[\left(C_0 - C_e / C_0\right)\right] * 100\% \tag{2}$$

where C_0 and C_e are MNZ concentrations at the start of the experiment and at equilibrium (mg/L), respectively.

2.3. Adsorption kinetics

Lagergren's pseudo-first-order rate equation [Eq. (3)] describes the adsorption of liquid-solid systems based on the concentration of the solution and adsorption capacity of the solid [22,23]. Eq. (4) depicts the expression for the pseudo-first-order model in a linearized form:

$$dq / dt = k_1\left(q_e - q_t\right) \tag{3}$$

$$\ln\left(q_e - q_t\right) = \ln q_e - k_1 t \tag{4}$$

where q_e and q_t are adsorption capacities (mg/g) at equilibrium and at various times (t), respectively. k_1 is the pseu-

do-first-order rate constant (min^{-1}) that was obtained by plotting a graph of vs. t.

The rate of pseudo-second-order reaction depends on the amount of adsorbed on the adsorbent [24]. The expressions for the pseudo-second-order model and the linearized form are given in Eqs. (5) and (6), respectively:

$$dp/dt = k_2\left(q_e - q_t\right)^2 \tag{5}$$

$$t/q_t = 1/\left(k_2 q_e^{\,2}\right) + t/q_t \tag{6}$$

where k_2 is the Pseudo-second-order rate constant (g/mg/min) and it was obtained by plotting a graph (t/q_t) vs. t.

2.4. Adsorption isotherms

The Langmuir and Freundlich isotherm were used for the analysis of experimental equilibrium isotherm data. The Langmuir isotherm model assumes that the adsorption is monolayer and takes place at specific homogeneous sites on the adsorbent [25]. The Langmuir isotherm is shown in Eq. (7):

$$q_e = q_m K_L C_e / \left(1 + K_L C_e\right) \tag{7}$$

where q_e is the equilibrium adsorption capacity (mg/g), q_m is the Langmuir isotherm constant representing monolayer adsorption capacity (mg/g), C_e is the equilibrium concentration of MNZ in the solution (mg/L) and K_L is the Langmuir constant. Eq. (8) shows the linearized form of the Langmuir isotherm:

$$C_e/q_e = 1/\left(K_L q_m\right) + C_e/q_m \tag{8}$$

The Langmuir isotherm constants, i.e., K_L and q_m, are obtained by plotting a graph of $1/q_e$ vs. $1/C_e$. Favorability of adsorption process is evaluated by a dimensionless parameter i.e., separation or equilibrium parameter (R_L), as shown in Eq. (9):

$$R_L = 1/\left(1 + K_L C_0\right) \tag{9}$$

If $0 < R_L < 1$, the adsorption process is favorable, $R_L > 1$ indicates that adsorption is unfavorable, $R_L = 1$ indicates linear adsorption and $R_L = 0$ indicates that the adsorption process is irreversible in nature.

The Freundlich isotherm [Eq. (10)] is an empirical expression based on the assumption that the adsorbent has a heterogeneous surface composed of different classes of adsorption sites [22,26]. This can be applied to multilayer adsorption, with a non-uniform distribution of adsorption heat and affinities over the heterogeneous surface [27].

$$q_e = K_F C_e^{\frac{1}{n}} \tag{10}$$

where K_f is the Freundlich isotherm constant signifying adsorption capacity and is the Freundlich constant representing intensity of the adsorption or surface heterogeneity, revealing higher heterogeneity as it tends to 0. The value of Freundlich constant between 0 and 1 indicates favorable adsorption. Eq. (11) shows the linearized form of Freundlich isotherm, and a plot of $\ln(q_e)$ vs. $\ln(C_e)$ gives slop and intercept K_F.

$$\ln(q_e) = \ln K_F + \frac{1}{n}\ln C_e \tag{11}$$

2.5. Thermodynamics

The magnitude of activation energy gives an idea about the type of adsorption which is mainly physical or chemical [28]. The physisorption processes usually have energy in the rangeof 5–40 kJ/mol while higher activation energy (40–800 kJ/mol) suggests chemisorption [29]. The activation energy E_a (kJ/mol) for MNZ adsorption is calculated by the Arrhenius equation:

$$\ln(K_d) = -\frac{E_a}{RT} + \ln A \tag{12}$$

The thermodynamic parameters have been studied to gain an insight into the adsorption behavior. The parameters including the change in free energy (ΔG), enthalpy (ΔH), and entropy (ΔS) are calculated according to the following equations:

$$K_d = q_e(W/V)/C_0 \tag{13}$$

$$\Delta G = -RT\ln(K_d) \tag{14}$$

$$\ln(K_d) = \Delta S/R - \Delta H/RT \tag{15}$$

where A is the Arrhenius factor, R is the universal gas constant (8.314 J/mol K), T is temperature (K), and K_d is the distribution coefficient for the adsorption. V is the volume of MNZ solution (L) and W is the mass of adsorbent (g).

3. Results and discussion

3.1. Characterization

SEM is widely used to study the morphological features and surface characteristics of the adsorbent materials [32,33]. In the present study, SEM is used to assess morphological changes in the ACFs surfaces following adsorption of the MNZ. The SEM images of the original ACF are shown in Fig. 2a and Fig. 2b. It can be seen that the ACFs present smooth and the structure is orderly and compact. From Fig. 2c, it can be seen that after ACFs adsorption showed a distinct roughness. The observed phenomenon also provided further evidence that the adsorption process involved MNZ adsorption in the ACFs surface. The previous studies [18–20] also showed that the external surface displayed more curved planes and holes after adsorption.

The pore structure and specific surface area of an adsorbent can be obtained by constructing an adsorption-desorption isotherms of the ACFs. It can be seen from Fig. 3a that the shape of the isotherm is type II isotherm according to the international union of pure and applied chemistry IUPC classification, which indicated the ACFs was a combination

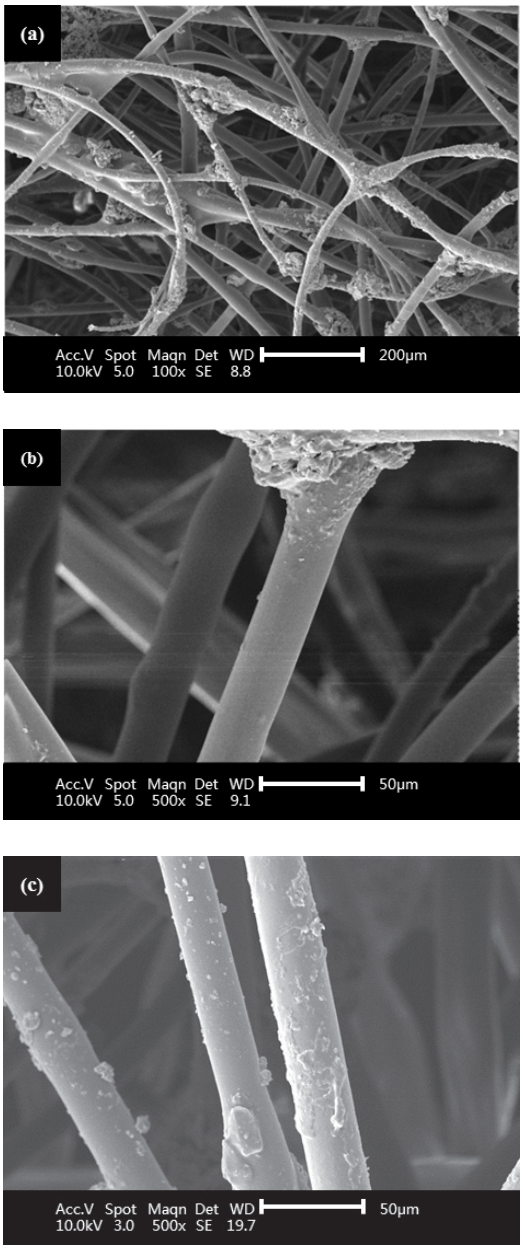

Fig. 2. SEM images of the ACFs (a , b) and after ACFs adsorption (c).

of mesopore. Fig. 3b presents the pore size distribution of the ACFs. The micropores volume was determined using BJH desorption branch and the pore size distribution was determined from the density functional theory. The peaks appeared at a wide range of pore width from 10 to 30 nm with the average pore size of 2.58 nm, which also indicated the existence of mesopore. The surface area of the ACF was found out to be 175.40 m^2/g with total pore volume of 0.35 cm^3/g.

3.2. Effect of pH

The pH parameter is essential in adsorption process because it can affect directly on ionization of adsorbent and

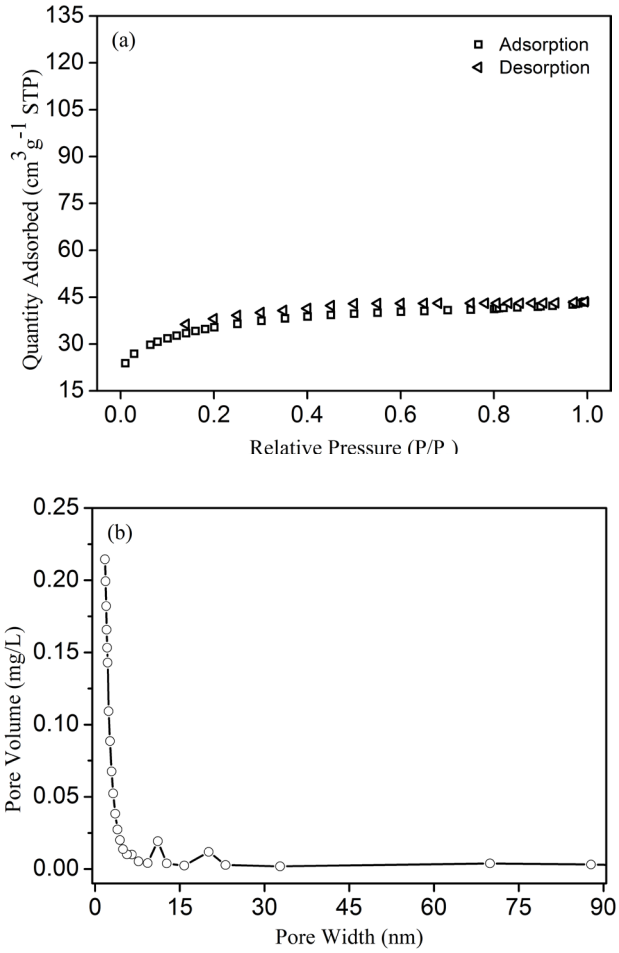

Fig. 3. N_2 adsorption/desorption isotherm (a) and pore size (b) distribution chart for the ACF.

adsorbate. Fig. 4 shows the variation of adsorption with different pH values at 298 K, 1.0 g of ACFs dose was and MNZ solution (10 mg/L, 20 mg/L, 30 mg/L concentration). While the pH of MNZ solution increased from 5 to 10, the adsorption of MNZ was not obvious. This results is consistent with Belhassen et al. [15] studies. This result can be explained by the fact that from *pKa* (metronidazole) = 2.6 only one from is present in the solution deprotonated [15,32]. Therefore, the following work on the adsorption will be studied under natural pH condition of the MNZ solution.

3.3. Effect of ACFs dose

The effect of the ACFs dose on the removal of MNZ solution (10 mg/L, 20 mg/L, 30 mg/L concentration) was studied with the adsorbent dose varying from amount of ACFs 0.2 g to 1.2 g/150 mL at 298 K. The study shows an enhancement in adsorption with the increase in dose of the ACFs. As seen in Fig. 5, when the dose of ACFs is increased from 0.2 g to 1.2 g, the adsorbed amount of MNZ increased from 0.53 mg/g to 1.32 mg/g for MNZ (10 mg/L), 1.52 mg/g to 2.48 mg/g for MNZ (20 mg/L) and 1.40 mg/g to 2.48 mg/g for MNZ (30 mg/L), respectively. So, it can be

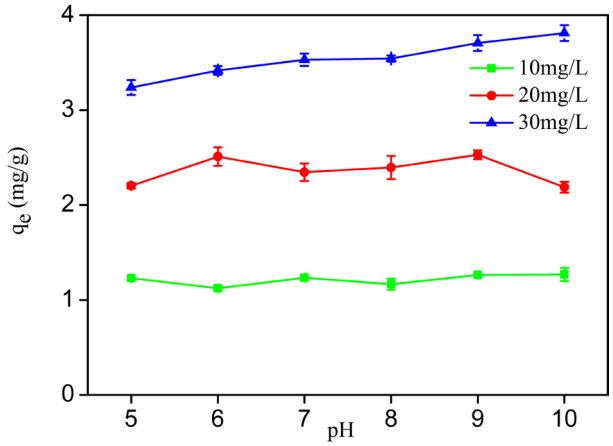

Fig. 4. Effect of varying pH on the MNZ adsorption rate for different concentrations (dose of ACFs 1.0 g, at 298 K).

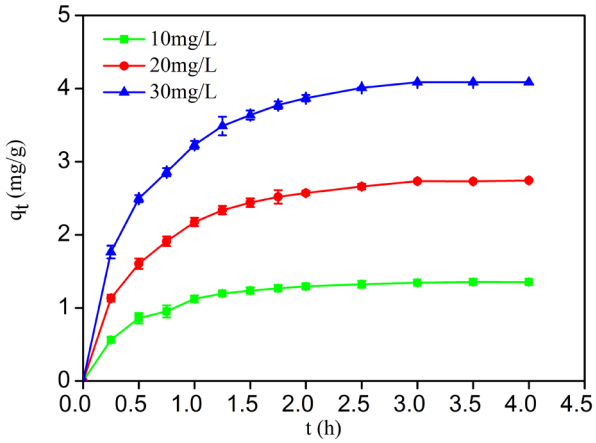

Fig. 6. Effect of contact time on the MNZ adsorption rate for different concentrations (dose of ACFs 1.0 g, pH 7.0, at 298 K).

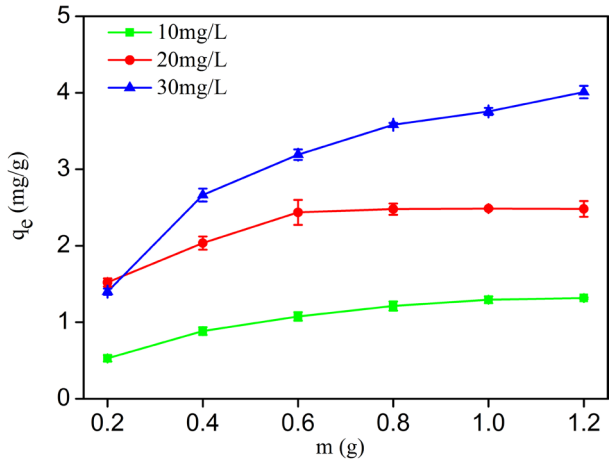

Fig. 5. Effect of dose of ACFs of the MNZ adsorption rate for different concentrations (pH 7.0, at 298 K).

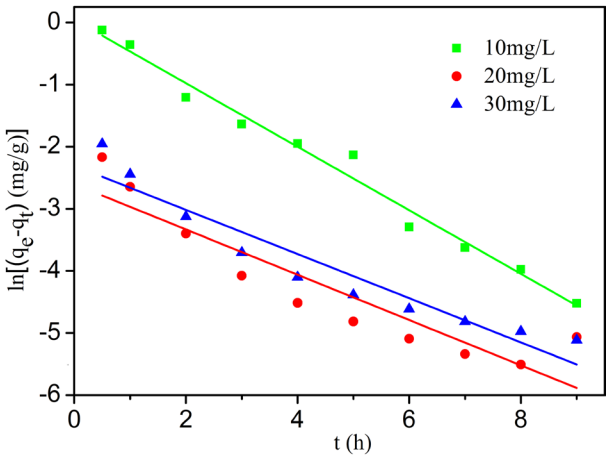

Fig. 7. Test of pseudo-first-order kinetic model for the adsorption of MNZ with different concentrations of ACFs composites (dose of ACFs 1.0 g, pH 7.0, at 298 K).

attributed to the greater availability of the active sites or surface area at higher doses of adsorbent. In this work, we choose the dose of ACFs was 1.0 g/L.

3.4. Adsorption kinetics

The effect of contact time (0–4 h) on the adsorption of MNZ with different concentrations of ACFs is shown in Fig. 6. The amounts of MNZ adsorbed on the ACFs (q_t, mg/g) increased rapidly in 30 min. It is also observed that the amounts increased continuously, but the rates became slowly with the increase of contact time and finally reached equilibrium after 1 h. This indicated that the MNZ adsorption on the ACFs is a fast process, and nearly 95% of adsorption takes place within 60 min.

In this study, the adsorption kinetics data are analyzed using two different kinetics models: Pseudo-first-order model and Pseudo-second-order model. The linear plots ln ($q_e - q_t$) vs. t and t/q_t vs. t for the MNZ with different concentrations on the ACFs are shown in the Figs. 7 and 8, respectively. The rate constant k, the calculated adsorp-

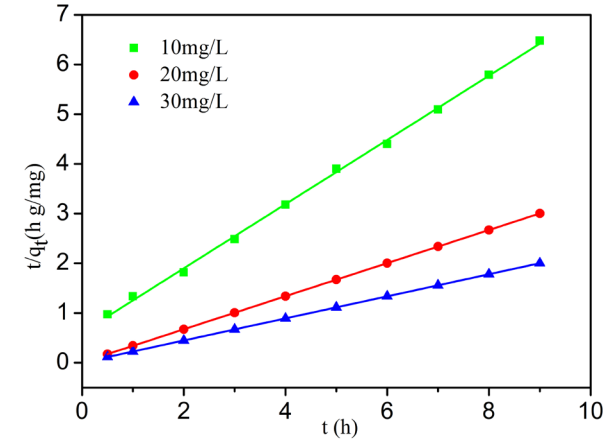

Fig. 8. Test of pseudo-second-order kinetic model for the adsorption of MNZ with different concentrations of ACFs composites (dose of ACFs 1.0 g, pH 7.0, at 298 K).

tion capacity $q_{e,cal}$ and the correlation coefficient R^2 for the pseudo-first-order model and pseudo-second-order model in the Table 1 and Table 2, respectively. It showed that the correlation coefficient for the pseudo-second-order model ($R^2 > 0.99$) was higher than the pseudo-first-order model ($R^2 > 0.87$). It was observed that the pseudo-second-order model was found to be fit well the data of the kinetic study.

3.6. Adsorption isotherms

The equilibrium isotherms at various temperatures were studied by varying the initial concentrations of MNZ under ACFs dose 1.0 g/150 mL. The constant of q_m, K_f, R^2 and n are given in Table 3. This table shows that the data with R^2 values were in the oder Langmuir > Freundlich. Thus, the higher R^2 value suggests that the Langmuir model fits well with the experimental data of MNZ adsorption was achieved by Langmuir isotherm represented by linear plot of C_e vs. C_e/q_e (Fig. 9). The values of n and K_f for Freundlich isotherm at various temperatures were determined from the slopes and intercepts of linear plots of ln C_e vs. ln q_e (Fig. 10). The equilibrium adsorption amount of MNZ increased from about 1.809 mg/g to 2.034 mg/g as the adsorption temperature increases from 25°C to 30°C, which indicated an endothermic adsorption process and increasing temperature favors the adsorption of MNZ on ACFs. This result revealed the homogeneous nature of MNZ adsorption on the carbon surface, as explained by Muthanna and Theydan [13,14] who showed the successful application of Langmuir isotherm to correlate adsorption isotherm data of metronidazole on activated carbon from Siris seed pods by microwave–induced KOH activation.

Table 1
Kinetic parameters of pseudo-first-order for the adsorption of MNZ with different concentrations of ACFs (dose of ACFs 1.0 g, pH 7.0, at 298 K)

	Pseudo-first-order			
C_0 (mg/L)	$q_{e,exp}$ (mg/L)	$q_{e,cal}$ (mg/L)	k_1 (1/min)	R^2
10	1.4	1.64592	0.957	0.9843
20	3.0	1.41807	1.6537	0.932
30	4.5	1.431324	1.9315	0.8701

Table 2
Kinetic parameters of pseudo-second-order for the adsorption of MNZ with different concentrations of ACFs (dose of ACFs 1.0 g, pH 7.0, at 298 K)

	Pseudo-second-order			
C_0 (mg/L)	$q_{e,exp}$ (mg/L)	$q_{e,cal}$ (mg/L)	k_2 (1/min)	R^2
10	1.4	1.870557	0.4551637	0.9961
20	3.0	1.7170329	1.04785	0.9979
30	4.5	2.56805	0.7020035	0.9979

Table 3
Parameters of Langmuir and Freundlich adsorption isotherm models for the MNZ on the ACFs (dose of ACFs 1.0 g, pH 7.0, 20 mg/L)

	Parameters	Temperature		
		25°C	30°C	35°C
Langmuir	q_m (mg/g)	1.8090	2.0342	1.8477
	K_L (L/mg)	3.8505	8.0086	4.6945
	R^2	0.9937	0.9950	0.9906
	R_L	0.0128	0.0008	0.1053
Freundlich	n	1.7960	2.7093	2.0442
	K_f (mg/g(L/mg)$^{1/n}$)	2.7857	3.6452	4.2010
	R^2	0.8340	0.8498	0.8044

3.7. Thermodynamics of ACFs adsorption

The Langmuir and Freundlich adsorption isotherm simulations were used to calculate the thermodynamic param-

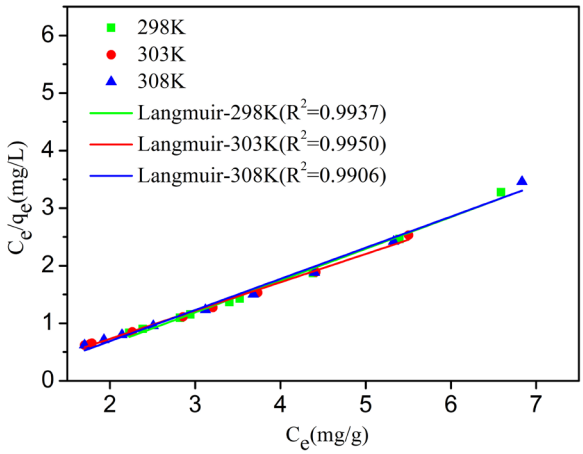

Fig. 9. Langmuir adsorption isotherms for the adsorption of the MNZ onto ACFs at different temperatures (dose of ACFs 1.0 g, pH 7.0).

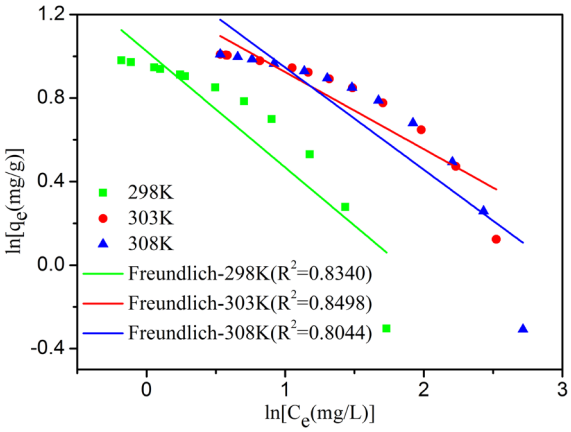

Fig. 10. Freundlich adsorption isotherms for the adsorption of the MNZ onto ACFs at different temperatures (dose of ACFs 1.0 g, pH 7.0).

eters of adsorption. The values of ΔH and ΔS have been calculated from the slope and intercepts of the linear plot of Eq. (13) represented by ln (K_d) vs. 1/T (Fig. 12). The value of E_a is obtained from the slope of linear plot for Arrhenius equation [Eq. (12)] represented by ln(k_2) vs. 1/T (Fig. 11). The values of ΔG are determined from Eq. (14) at each temperature. It can be seen from Table 4, The values of Gibbs free energy (ΔG) were –10.8435, –15.8751, –17.4143 kJ/mol at temperatures of 298 K, 303 K and 308 K. The negative ΔG values indicated spontaneous nature of the adsorption of MNZ antibiotic [33]. The decrease in ΔG values with increasing temperature suggested that higher temperature made the adsorption easier [34]. The value of enthalpy variation (ΔH) obtained in this study was 10.8435 kJ/mol. Positive ΔH showed the endothermic nature of MNZ adsorption [35]. Thus, according to the values of Ea (higher than 40 kJ/mol) and ΔH, the adsorption of MNZ has taken place via chemisorption [36]. About 60% of the *C* in ACFs exists in the form of graphite-like carbon, and more than 50% of the carbon atoms are located on the internal and external surfaces [37–39]. Due to the unsaturation of carbon atoms on the surface, it can combine with other atoms and atomic groups in a chemical form, thus forming a unique surface chemical structure [40,41]. The positive entropy variation (ΔS) value indicated the increased randomness in the interface during the adsorption process.

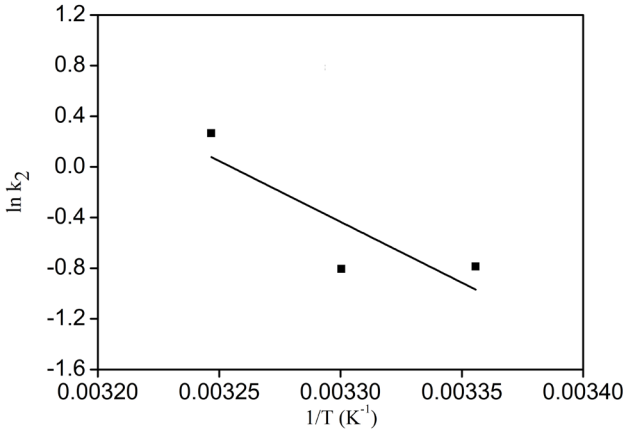

Fig. 11. Plot of ln k_2 versus 1/T for MNZ adsorption (dose of ACFs 1.0 g, pH 7.0).

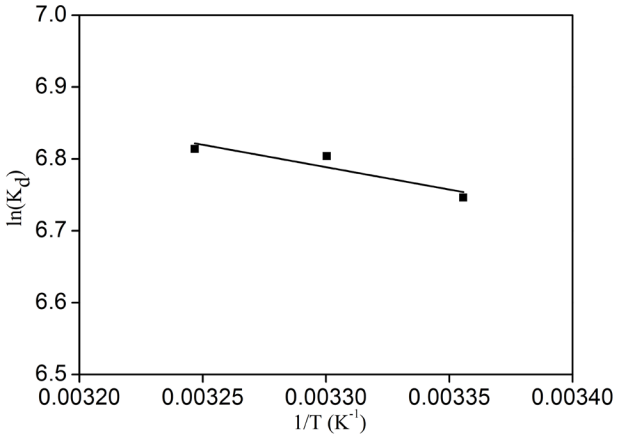

Fig. 12. Plot of ln(K_d) versus 1/T for MNZ adsorption (dose of ACFs 1.0 g, pH 7.0).

Table 4
Activation energy and thermodynamic parameters

E_a (kJ/mol)	ΔH (kJ/mol)	ΔS (kJ/mol)	–ΔG (kJ/mol)		
			298K	303K	308K
66.0300	10.8435	0.2518	10.8435	15.8751	17.4143

4. Conclusion

The paper presented the activated carbon fiber adsorption metronidazole solution at different pH, temperature and dose of activated carbon fiber. The adsorption kinetic data were well described by the pseudo-second order model, Langmuir adsorption isotherm models and thermodynamic analysis showed that the adsorption of metronidazole was endothermic and spontaneous under studied conditions.

Acknowledgements

This work was supported by the Natural Science Foundation and Technology Department of Jilin province, China (20150101093C) and Technology Department Key research of Jilin province, China (20140204038SF).

References

[1] C. Mahugo-Santana, Z. Sosa-Ferrera, M.E. Torres-Padrón, J.J. Santana-Rodríguez, Analytical methodologies for the determination of nitroimidazole residues in biological and environmental liquid samples: a review, Anal. Chim. Acta, 665(2) (2010) 113–122.
[2] I. Sirés, E. Brillas, Remediation of water pollution caused by pharmaceutical residues based on electrochemical separation and degradation technologies: a review, Environ. Int., 40 (2012) 212–229.
[3] Z. Fang, J. Chen, X. Qiu, X. Qiu, W. Cheng, L. Zhu, Effective removal of antibiotic metronidazole from water by nanoscale zero-valent iron particles, Desalination, 268(1–3) (2011) 60–67.
[4] R.F. Dantas, O. Rossiter, A.K.R. Teixeira, A.S.M. Simões, V.L. da Silva, Direct UV photolysis of propranolol and metronidazole in aqueous solution, Chem. Eng. J., 158(2) (2010) 143–147.
[5] A. Bendesky, D. Menéndez, P. Ostrosky-Wegman, Is metronidazole carcinogenic?, Reviews. Mutat. Res., 511(2) (2002) 133–144.
[6] M. Klavarioti, D. Mantzavinos, D. Kassinos, Removal of residual pharmaceuticals from aqueous systems by advanced oxidation processes, Environ. Int., 35(2) (2009) 402–417.
[7] M.J. Gómez, M. Petrović, A.R. Fernández-Alba, D. Barceló, Determination of pharmaceuticals of various therapeutic classes by solid-phase extraction and liquid chromatography–tandem mass spectrometry analysis in hospital effluent wastewaters, J. Chromatography A, 1114(2) (2006) 224–233.
[8] D.K. Bempong, R.G. Manning, T. Mirza, L. Bhattacharyya, A stability-indicating HPLC assay for metronidazole benzoate, J. Pharm. Biomed. Anal., 38(4) (2005) 776–780.

[9] S.V. Manjunath, S.M. Kumar, H.H. Ngo, W. Guo, Metronidazole removal in powder-activated carbon and concrete-containing graphene adsorption systems: Estimation of kinetic, equilibrium and thermodynamic parameters and optimization of adsorption by a central composite design, J. Environ. Sci. Health, Part A, 52(14) (2017) 1269–1283.
[10] A. Lam, A. Rivera, G. Rodríguez-Fuentes, Theoretical study of metronidazole adsorption on clinoptilolite, Micropor. Mesopor, Mater., 49(1–3) (2001) 157–162.
[11] M.B. Johnson, M. Mehrvar, Aqueous metronidazole degradation by UV/H_2O_2 process in single-and multi-lamp tubular photoreactors: kinetics and reactor design, Ind. Eng. Chem. Res., 47(17) (2008) 6525–6537.
[12] H. Ding, G. Bian, Adsorption of metronidazole in aqueous solution by Fe-modified sepiolite, Desal. Water Treat., 55(6) (2015) 1620–1628.
[13] M.J. Ahmed, S.K. Theydan, Microwave assisted preparation of microporous activated carbon from Siris seed pods for adsorption of metronidazole antibiotic, Chem. Eng. J., 214 (2013) 310–318.
[14] M.J. Ahmed, S.K. Theydan, Microporous activated carbon from Siris seed pods by microwave-induced KOH activation for metronidazole adsorption, J. Anal. Appl. Pyrol., 99 (2013) 101–109.
[15] H. Belhassen, I. Ghorbel-Abid, L. Rim, Removal of metronidazole from aqueous solution using activated carbon, Eur. J. Chem., 8(3) (2017) 310–313.
[16] E.M. Kalhori, T.J. Al-Musawi, E. Ghahramani, H. Kazemian, M. Zarrabi, Enhancement of the adsorption capacity of the light-weight expanded clay aggregate surface for the metronidazole antibiotic by coating with MgO nanoparticles: Studies on the kinetic, isotherm, and effects of environmental parameters, Chemosphere, 175 (2017) 8–20.
[17 E. Çalışkan, S. Göktürk, Adsorption characteristics of sulfamethoxazole and metronidazole on activated carbon, Separ. Sci. Technol., 45 (2010) 244–255.
[18] D. Zhou, R. Hai, W. Wang, D. Zhao, S. Wang, Activated carbon fiber filler in aerated bioreactor for industrial wastewater treatment, Water Sci. Technol., 65(10) (2012) 1753–1758.
[19] C.M. Du, D.W. Huang, H.X. Li, M.D. Xiao, K. Wang, L. Zhang, Z.Y. Lu, T.F. Chen, J.M. Mo, D. Gao, Y.H. Huang, S.K. Liu, L. Yu, C.R. Zhang, Adsorption of acid orange II from aqueous solution by plasma modified activated carbon fibers, Plasma Chem. Plasma Process., 33(1) (2013) 65–82.
[20] S. Wang, X. Li, H. Zhao, X. Quan, S. Chen, H. Yu, Enhanced adsorption of ionizable antibiotics on activated carbon fiber under electrochemical assistance in continuous-flow modes, Water Res., 134 (2018) 162–169.
[21] J.-E. Gu, G. Son, H. Lee, J. Park, Y.-N. Kwon, S. Lee, Improved water quality and phenol degradation via a combination of electron-beam irradiation (EBI) and activated carbon fiber (ACF), Desal. Water Treat., 64 (2017) 118–126.
[22] S. Lagergren, Zurtheorie der sogenannten adsorption geloster-stoffe. Kungligasvenskavetenskapsakademiens. Handlingar, 24 (1898) 1–39.
[23] Y.S. Ho, G. McKay, Pseudo-second order model for sorption processes, Process Biochem., 34(5) (1999) 451–465.
[24] W.J. Weber, J.C. Morris, Kinetics of adsorption on carbon from solution, J. Sanit. Eng. Div., 89(2) (1963) 31–60.
[25] I. Langmuir, The constitution and fundamental properties of solids and liquids. Part I, Solids. J. Amer. Chem. Soc., 38(11) (1916) 2221–2295.
[26] H. Freundlich, Über die adsorption in lösungen, Z. Physikalische Chemie, 57(1) (1907) 385–470.
[27] H. Freundlich, W. Heller, The adsorption of cis-and trans-azobenzene, J. Amer. Chem. Soc., 61(8) (1939) 2228–2230.
[28] Z. Belala, M. Jeguirim, M. Belhachemi, F. Addoun, G. Trouvé, Biosorption of basic dye from aqueous solutions by date stones and palm-trees waste: kinetic, equilibrium and thermodynamic studies, Desalination, 271 (2011) 80–87.
[29] T.S. Anirudhan, P.G. Radhakrishnan, Thermodynamics and kinetics of adsorption of Cu(II) from aqueous solutions onto a new cation exchanger derived from tamarind fruit shell, J. Chem. Thermodyn., 40(4) (2008) 702–709.
[30] S. Gupta, A. Pal, P.K. Ghosh, M. Bandyopadhyay, Performance of waste activated carbon as a low-cost adsorbent for the removal of anionic surfactant from aquatic environment, J. Environ. Sci. Health, Part A, 38(2) (2003) 381–397.
[31] B. Tansel, P. Nagarajan, SEM study of phenolphthalein adsorption on granular activated carbon, Adv. Environ. Res., 8(3–4) (2004) 411–415.
[32] H. Ding, G. Bian, Adsorption of metronidazole in aqueous solution by Fe-modified sepiolite, Desal. Water Treat., 55(6) (2015) 1620–1628.
[33] H. Guedidi, L. Reinert, Y. Soneda, N. Bellakhal, L. Duclaux, Adsorption of ibuprofen from aqueous solution on chemically surface-modified activated carbon cloths, Arab. J. Chem., 10 (2017) S3584–S3594.
[34] A.M. Aljeboree, A.N. Alshirifi, A.F. Alkaim, Kinetics and equilibrium study for the adsorption of textile dyes on coconut shell activated carbon, Arab. J. Chem., 10 (2017) S3381–S3393.
[35] Y. Yu, Y.Y. Zhuang, Z.H. Wang, M.-Q. Qiu, Adsorption of water-soluble dyes onto modified resin, Chemosphere, 54(3) (2004) 425–430.
[36] H.N. Tran, S.J. You, H.P. Chao, Thermodynamic parameters of cadmium adsorption onto orange peel calculated from various methods: a comparison study, J. Environ. Chem. Eng., 4(3) (2016) 2671–2682.
[37] J. Li, D.H.L. Ng, P. Song, C. Kong, Y. Song, P. Yang, Preparation and characterization of high-surface-area activated carbon fibers from silkworm cocoon waste for Congo red adsorption, Biomass Bioenergy, 75 (2015) 189–200.
[38] L. Wang, Y. Yao, Z. Zhang, L. Sun, W. Lu, W. Chen, H. Chen, Activated carbon fibers as an excellent partner of Fenton catalyst for dyes decolorization by combination of adsorption and oxidation, Chem. Eng. J., 251 (2014) 348–354.
[39] G.B. Baur, O. Beswick, J. Spring, I. Yuranov, L. Kiwi-Minsker, Activated carbon fibers for efficient VOC removal from diluted streams: the role of surface functionalities, Adsorption, 21(4) (2015) 255–264.
[40] F. Zhou, C. Lu, Y. Yao, L. Sun, F. Gong, D. Li, K. Pei, W. Lu, W. Chen, Activated carbon fibers as an effective metal-free catalyst for peracetic acid activation: Implications for the removal of organic pollutants, Chem. Eng. J., 281 (2015) 953–960.
[41] C. Brasquet, B. Rousseau, H. Estrade-Szwarckopf, P. Le Cloirec, Observation of activated carbon fibres with SEM and AFM correlation with adsorption data in aqueous solution, Carbon, 38(3) (2000) 407–422.